Optimal Performance Evaluation of Thermal AGC Units based on Multi-dimensional Feature Analysis

Bin Li[a], *Senior Member, IEEE*, Shuai Wang[a]*, Botong Li[a]*, Hongbo Li[b], Jianzhong Wu[c]

[a] The Key Laboratory of Smart Grid of Ministry of Education, Tianjin University, Tianjin 300072, China
[b] Power Dispatching and Control Center, Inner Mongolia Power (Group) Co., Ltd, Hohhot 010020, China
[c] School of Engineering, Cardiff University, Cardiff CF24 3AA, UK

***Abstract*: In modern energy system, automatic generation control (AGC) is the core technology of real-time output regulation for thermal power generator. The performance of thermal AGC units must be accurately evaluated to measure their actual contribution to the energy system. However, based on current conventional evaluation methods, the difficulty of the tasks undertaken by AGC units has not been distinguished and quantified. An optimal performance evaluation method based on multi-dimensional feature analysis is proposed. Firstly, a performance index describing the difference between the expected regulating energy and the actual regulated energy of AGC units is designed, which improves the universality of the evaluation to the actual engineering scenarios. Additionally, after data preprocessing and data cleaning, a sample space is constructed to significantly distinguish the difficulty of tasks performed by AGC units. Finally, a multi-dimensional feature analysis in the sample space is proposed to find the optimal performance points of AGC units. Based on historical data, the proposed methods were verified on real AGC units. The experimental results show that the proposed method obtains detailed evaluation results of thermal AGC units with different control requirements and solves the problem of evaluation failure in traditional method.**

***Keywords:* automatic generation control, performance evaluation, sample space, feature analysis, optimal dynamic performance**

1. Introduction

As an essential energy source, thermal power generation is widely used in the energy systems all over the world. The components of modern energy systems have become increasingly complex. The strong random disturbance issues caused by the large-scale grid connections of distributed energy, such as wind energy, photovoltaic energy storage and electric vehicles, must be resolved[1], and the actual contributions of various energy sources must be accurately evaluated[2]. For energy systems, electrical frequency is one of the important indicators to measure the quality of energy supply. When the energy generation and load are unbalanced, the electrical frequency fluctuates, which affects the operation of industrial users and power plants, and even leads to large-scale blackouts[3]. The frequency should be maintained within a permissible band around a nominal value, typically 50Hz or 60 Hz. Modern engineers and researchers use state-of-the-art communication technologies, signal processing, and data analysis techniques to offer operators enhanced system insight, including detection of sudden frequency deviations[4].

In large-scale energy systems, Automatic Generation Control (AGC) is one of the important technologies to maintain the electrical frequency stability and ensure the balance between load and energy supply[5]. AGC can be normally divided into two procedures: (a) The total power references tracking of AGC, and (b) the total power references dispatch into each unit through optimization[6]. When the electrical frequency fluctuates, the energy dispatch center sends several dynamic instructions to energy units equipped with AGC system to increase or decrease their output, thus restoring the desired electrical frequency of the energy system[7]. In the energy trading market, in order to ensure the high quality of energy supply, the performance of AGC units must be strictly evaluated[8]. If the energy output is not effectively adjusted, AGC units will receive economic punishment. Furthermore, the electrical frequency deviation may further deteriorate and even lead to the collapse of the energy supply[9].

In modern energy systems, power sources such as thermal plants, photovoltaic and hydropower units have different characteristics, which lead to unsatisfactory performances with the traditional AGC strategy, especially the frequency instability, therefore, more effective AGC strategies are awaiting to be developed[10]. In order to secure the safe operation of the energy system, the output of AGC units must be stable and controllable. The output of wind and solar energy usually shows strong randomness, which is difficult to meet the requirements[11]. Furthermore, realistic models of renewable energy sources are developed, but they are limited to isolated systems only[12]. Hydropower is often used as AGC units due to fast response, but

This work was supported by Science and Technology Project of State Grid Corporation of China (5600-202046347 A-0-0-00). (*Corresponding author: Shuai Wang, Botong Li.*)

Bin Li, Shuai Wang, Botong Li are with the Key Laboratory of Smart Grid of Ministry of Education, Tianjin University, Tianjin 300072, China (e-mail: binli@tju.edu.cn; namewangs@tju.edu.cn; libotong@tju.edu.cn).

Hongbo Li is with Power Dispatching and Control Center, Inner Mongolia Power (Group) Co., Ltd, Hohhot 010020, China (hbli_tju@126.com)

Jianzhong Wu is with School of Engineering, Cardiff University, Cardiff CF24 3AA, UK (e-mail: wuj5@cardiff.ac.uk)

its performance is often limited by seasonal flood and drought[13]. Nuclear power usually operates at full power, and it is difficult to ensure safety if complex AGC instructions are received[14]. Battery energy storage system is usually considered as one of the perfect AGC units, but the frequent charging and discharging caused by AGC instructions means high maintenance investment[15]. In contrast, thermal energy provides large-scale stable generation, which is not affected by seasons and climate[16]. Most thermal power units are equipped with AGC system, and undertake most of the energy control tasks in the daily operation[17]. Therefore, the performance evaluation of thermal AGC units is a very important work of the energy system.

AGC service is a paid auxiliary energy service obtained from power plants by Independent System Operators (ISO)[18]. ISO in different regions have implemented specific evaluation indicators for the AGC units. Typical examples include the European power market regulated by Union for the Co-ordination of Transmission of Electricity (UCTE)[18], the Pennsylvania-NewJersey-Maryland (PJM) power market and Midcontinent Independent System Operator (MISO) power market regulated by the Federal Energy Regulatory Commission (FERC)[20], and the State Grid Corporation of China (SGCC) power market and China Southern Power Grid (CSG) power market regulated by the National Energy Administration of China (NEAC)[21]. The specific evaluation methods in the above markets are described in [22] for North America, [23] for China, [24][25] for Germany, and [26] for Spain. In Section 2, the differences of different power market rules are illustrated in detail. In order to realize fast AGC power dispatching and optimal coordinated control of microgrids, researchers have proposed relevant methods in recent years. In [27], a virtual generation ecosystem control (VGEC) strategy is proposed, which adopts the idea of time tunnel and the principle of a new win-loss criterion. In [28], an automatic generation control method considering the uncertainties of key parameters (such as system inertia and load damping factors) is proposed. In the study of [29], the optimal automatic generation control of two area interconnected power system is considered, and the parameters of controllers were developed by simulated annealing (SA) techniques to obtain the best dynamic performance. For modeling economic dispatch with dynamic AGC constraints, the research of [30] proposes a flexibility management framework which can be solved by conducting reformulation and decomposition, and further proposes seven system flexibility indicators to reflect the system flexibility. In [31], an automatic generation control strategy based on Leader Harris Hawks Optimization (MPC-LHHO) algorithm is proposed for the regulation of frequency and voltage in renewable penetrated power systems. The proposed MPC-LHHO algorithm has been evaluated in coordination with the capacitive energy storage and virtual inertia units.

However, in the above conventional evaluation methods, the difficulty of the instructions received by AGC units has not been distinguished. The performance of different units varies due to the influence of service time, equipment health, and types of coal[32]. Although the AGC system concert can be heightened by the solicitation of soft computing approaches by setting of controller parameters, different units show different characteristics even under the same AGC instructions[33].

The research on thermal AGC unit optimal performance evaluation is not abundant in recent years. Only a few studies have proposed relevant improvements to the general performance evaluation. In [34], in order to further highlight the output characteristics of AGC units, the historical data were analyzed in time and frequency domain respectively. But in signal extraction, it assumes that the output of AGC units is a piecewise linear signal, and the actual output characteristics are inevitably lost. In the actual power generation data, the output of AGC units is nonlinear, and the accurate performance evaluation should conform to the actual situation as much as possible. The study in [35] points out that, in the energy trading market, the effect of AGC response delay must be considered, and the delay characteristics are different due to the nonlinear parameter of the AGC system. However, for large-scale energy system, it is a heavy work to accurately model all parameters of each AGC unit. A large amount of historical data is stored in the dispatching center, and the regularity of each unit can be fully described through data mining. In addition, the research shows that the response delay is not only affected by the factory parameters of the generation equipment, but also mainly depend on the resolution of the AGC instructions issued by the dispatch center. Therefore, AGC instructions must be preprocessed in performance evaluation. In [36], a generic modeling method for quality of AGC service is proposed. The time series error between the unit output and the set-point power is defined, and the error is scaled accordingly for different economic rules. However, the study used simulated data to evaluate AGC services, and some special cases in actual data were not verified. The actual AGC operation data was used and verified in [37]. In this study, the time series of the unit output were divided into short straight lines, and the performance of AGC unit is evaluated by comparing the amplitude changes of the divided lines and set-point power. Such an idea stems from the assumption that an AGC unit maintains a relatively stable upward or downward trend for a certain period of time. The method requires that the sampling window of the analyzed data should not be less than 5min, otherwise it is difficult to distinguish any features of the unit output. However, it is very common for the dispatch center to change the instructions within 5 minutes, and AGC performance evaluation is required to be completed in a shorter time.

According to the above conventional methods, either the simulated data is used, or the actual data is assumed to be linear, or a long sampling window is required, and it is worth noting that the difficulty of AGC tasks are also ignored. In other words, a data driven evaluation method for AGC units has not been proposed. In general, regularities are hidden in a large number of operating data. Therefore, it makes sense to analyze the historical data to achieve an accurate evaluation of AGC units. This paper proposes a performance evaluation method of thermal AGC units based on multi-dimensional feature analysis. The contributions of this paper are as follows:

- A performance index based on energy regulation was proposed, which accurately describes the tracking ability of

thermal AGC units, and the actual contribution of AGC units in the energy system is reflected.

- The concept of AGC sample space was proposed, focusing on the fusing of output amplitude, duration and tracking error of AGC units. The regularities of AGC operation data are analysed in a data-driven way.
- A method of searching the optimal performance of AGC units was proposed, and the appropriate operating conditions for different AGC units was obtained. The evaluation results are conducive to optimizing energy dispatching decisions.

The rest of this paper is organized as follows. Section 2 introduces the fundamental of thermal power units and AGC system, and illustrates the conventional methods in typical power systems. In continuation, Section 3 describes the performance evaluation method of thermal AGC units based on multi-dimensional feature analysis. Section 4 presents the experimental results and related analyses. Section 5 depicts the final conclusions.

2. Operational characteristics and conventional evaluation of automatic power generation control

Generally, AGC includes four aspects: control object, control target, control parameter and control effect[38]. First, the control object of AGC is the thermal power generation unit. It is mainly composed of two parts: coal-burning subsystem and water-steam subsystem. The schematic diagrams of the two subsystems are shown in Fig 1.

As shown in Fig 1(a), coal is ground into coal dust by a coal mill, and then mixed with hot air and blown into the boiler. After combustion, coal dust turns into fume and slag, which are sent to the atmosphere and the ash yard through the dust remover and the ash sluicing water respectively. In the process of coal-burning, the combustion efficiency of the boiler depends on the quality of the coal, as well as the quality of the coal mill and the hot air supply system.

As shown in Fig 1(b), the boiler generates steam by heating the feedwater, and the steam drives the turbine to rotate, which in turn rotates the generator. The electricity produced by the generator is fed into the power grid. After passing through the turbine, the steam becomes exhaust, which is condensed and circulated into the boiler together with the demineralized and deaerated raw water.

When the balance between the power supply and demand is broken, the frequency of the power grid fluctuates, which in turn affects the speed of the generator. Since the turbine is coaxial with the generator, the rotational speed of the turbine is also changed. In this situation, the AGC changes the turbine speed by increasing or decreasing the opening of the turbine inlet valve to restore the desired frequency of the power grid.

Therefore, the control object of AGC is a complex closed-loop nonlinear control system with multiple inputs and multiple outputs, resulting in different operating results under different operating conditions and different control purpose.

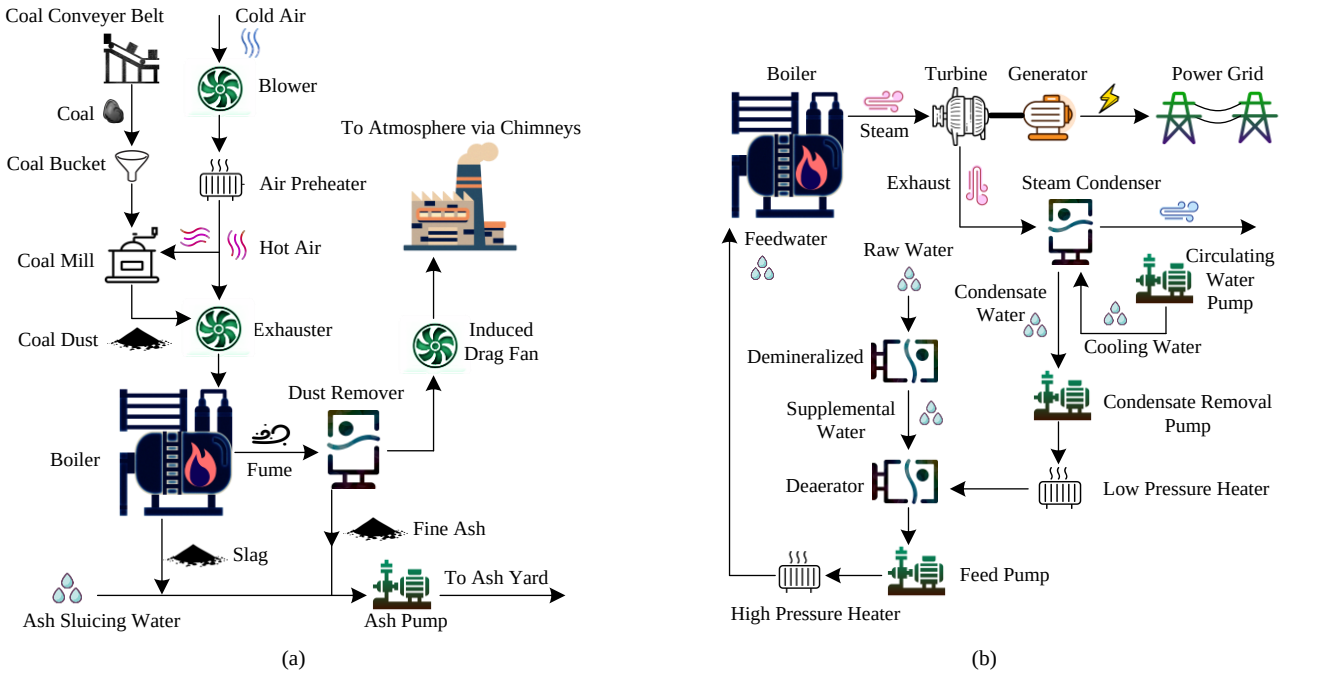

Fig. 1. A typical operation process of thermal power generation: (a) The coal-burning subsystem, (b) The water-steam subsystem.

The control target of AGC is to meet the real-time balance of power supply and demand under the premise of achieving high-quality power supply.

A schematic diagram of the control target of AGC is shown in Fig 2. Different AGC units receive different power set-point (P_{SET}) from the dispatch center, and each AGC unit adjusts its own active power output (P_{OUT}) to track P_{SET} as closely as possible. Both P_{SET} and P_{OUT} are sequential, where P_{SET} is a dynamically changing step signal and P_{OUT} is a nonlinear signal.

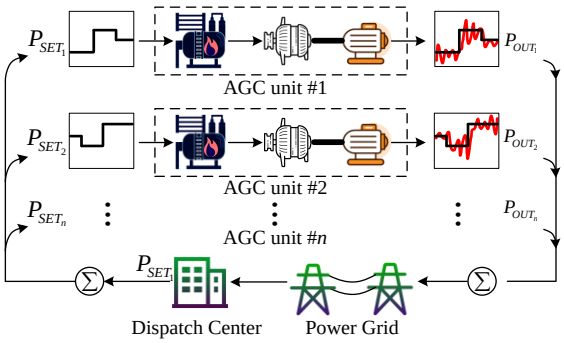

Fig. 2. The schematic diagram of the control target of AGC.

The control parameters of the AGC are determined by the Area Control Error (*ACE*)[39], which reflects the real-time deviation of power supply and demand in a regional power grid. *ACE* consists of two parts: the deviation between the actual frequency of the power grid and the target frequency, and the deviation between the actual active power in the tie line and the target active power. *ACE* is defined as Eq (1).

$$ACE = -10B(f - f_0) + (P - P_0) \tag{1}$$

where B is the regional frequency deviation coefficient (MW/0.1Hz). f is the measured frequency (Hz), and f_0 is the target frequency. P is the actual active power of the alternating current tie line between regions, and P_0 is the target active power between regions. The sending area is positive, and the receiving area is negative.

According to the P_{SET} dynamic allocation algorithm, the dispatch center allocates independent P_{SET} to different AGC units to minimize *ACE* to zero as much as possible[40]. However, from the point of view of the power grid, the control process does not consider the individual differences of units, and the AGC performance of units with certain parameters is considered to be completely stable.

The control effect of AGC on a single unit is reflected in the tracking ability of unit output to P_{SET}, which is also called dynamic performance. Four typical dynamic performance of different units under different P_{SET} are shown in Fig 3. Each subfigure in Fig 3 is a screenshot of historical data, from real AGC units, and the length of the screenshot window is 30 minutes.

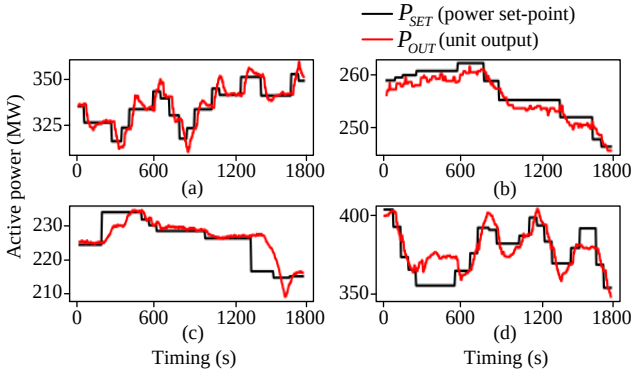

Fig. 3. Typical dynamic performance of different AGC units: (a) Overshoot regulation, (b) Loss of precision, (c) Output delay, (d) Reverse regulation.

As shown in Fig 3(a), whenever the unit receives a new P_{SET} step, the output of the unit always crosses the P_{SET} to form a corresponding upward or downward overshoot spike. This is mainly caused by the inertia of the unit output, and to a certain extent, it is also caused by the reversal of the P_{SET}. Fig 3(b) shows the loss of precision. The output of the unit does not stabilize around P_{SET} during the period when P_{SET} remains constant. Fig 3(c) shows the output delay. When the unit receives a large P_{SET} step, the unit output does not respond in time. Fig 3(d) shows the reverse regulation, that is, in some periods, the unit output does not increase or decrease correspondingly with P_{SET}, and even changes in the opposite direction, which is a typical undesired regulation.

AGC is described from above four aspects, including control object, control target, control parameter and control effect. It is obvious that, for a complex nonlinear control like AGC, multiple outputs do not strictly follow the causal mapping from multiple inputs, and the dynamic performance of a single unit usually exhibits a certain fuzzy tendency. Obviously, accurately describing the tracking ability of P_{OUT} to P_{SET} is the key to evaluating the performance of AGC units.

For the conventional AGC evaluation methods, there are mainly two types, one is the "permitted-band" method used in Europe (such as Spain and Germany), and the other is the "regulation mileage" method used in the United States and China, as shown in Fig 4.

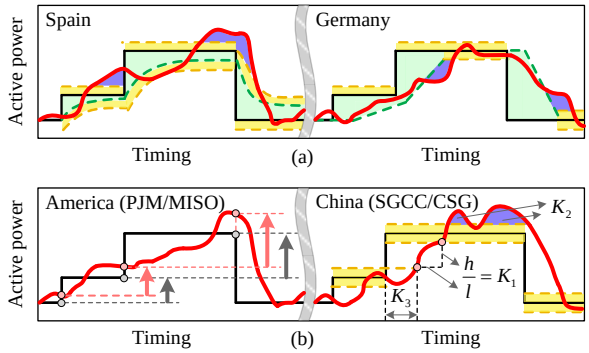

Fig. 4. Conventional AGC dynamic performance evaluation in power grid: (a) Spain and Germany, (b)America (PJM and MISO power market) and China (SGCC and CSG power market).

Fig 4(a) shows the "permitted-band" evaluation method in Spain and Germany respectively. The solid red line is P_{OUT}. The solid black line is P_{SET}, which represents the required ideal performance of the unit, so it is also called the fastest permitted response. Correspondingly, the dashed green line is the slowest permitted response[26]. For the power grid in Spain, the slowest permitted response nearly equal to a first-order exponential curve with a time constant of 100 seconds. In the German power grid, an initial response delay of 30 seconds is permitted after the unit has received a new P_{SET} step, and each P_{SET} step must be fully completed within 300 seconds. So the slowest permitted response in Germany is a straight line with a slope equal to the step value of the current P_{SET} divided by 270 seconds[25].

In Fig 4(a), the light green area between the dashed green line and the P_{SET} is the permitted response band. In addition, the dashed yellow line is the error tolerance boundary, which is generally a percentage of P_{SET} or a certain value (e.g. ±5%P_{SET} in Europe, ±2MW in China) [24]. The light yellow area between the dashed yellow line (error tolerance boundary), the dashed green line (slowest permitted response) and the P_{SET} is the error

tolerance band. The behavior of the unit's P_{OUT} exceeding the error tolerance band is unexpected and will be subject to financial penalties, corresponding to the purple area in Fig 4. For some special units that habitually have an offset between P_{SET} and P_{OUT}, strictly limiting the "permitted-band" may ignore the actual contribution of the unit to the power grid. For example, as mentioned in Fig 3(b), it is visible that the unit does not meet the strict requirements of the "permitted-band" due to loss of precision. However, the actual change of the unit output has achieved the general change of P_{SET}, which is still beneficial to the entire power grid. Hence the other method called "regulation mileage" overcomes this evaluation problem.

Fig 4(b) shows the "regulation mileage" evaluation method in the United States and China respectively. The adjustment mileage is equal to the absolute value of the difference between the output of the AGC unit at the beginning and the end of each P_{SET}. As illustrated in Fig 4(b) left, in American power grid, each pair of black and red arrows represents the required regulation mileage and the actual regulation mileage, respectively[22]. Here it is assumed that the movement towards the P_{SET} is positive, movement away from the P_{SET} is negative. It grants full remuneration if the actual regulation mileage is more than 70% of the required regulation mileage during 5-minute dispatch interval.

As illustrated in Fig 4(b)-right, based on the regulation mileage, for Chinese power grid, three indicators K_1, K_2 and K_3 are refined and proposed[23]. K_1 represents regulation speed, which is the gradient of P_{OUT} from crossing the current error tolerance boundary to reaching a new error tolerance boundary. K_2 represents regulation deviation, which is the area between P_{OUT} and the error tolerance boundary after P_{OUT} enters the error tolerance band for the first time. K_3 represents response delay, which is the time required for the unit to cross the error tolerance boundary for the first time after receiving the P_{SET}.

Since the P_{SET} is a dynamically changing step signal, the amplitude and duration of each step are dynamically changed. For conventional evaluations methods shown in Fig 4, the step duration and step amplitude of each P_{SET} are not considered. It means that the dynamic performance differences of AGC units under different regulation tasks are ignored. It is essential for the dispatch center to evaluate each AGC unit with different P_{SET} and then optimize the P_{SET}. In this context, an AGC dynamic performance evaluation method based on multi-dimensional feature analysis is proposed.

3. AGC dynamic performance evaluation based on multi-dimensional feature analysis

3.1. AGC-related data preprocessing

The dispatch center updates the P_{SET} automatically according to the ACE requirements. In order to mining the performance characteristics of different AGCs, the historical data of the inputs P_{SET} and outputs P_{OUT} must be preprocessed to construct the sample space of AGC performance. There are some special circumstances must be concerned, such as working mode the AGC unit, dead-band of the P_{SET} and impact of primary frequency control, etc.

First, when the ACE of an area meets the requirements of the power grid, the AGC unit may switches to the "Off-regulation" mode and does not undertake any frequency regulation task. Under this condition, the unit only provide basic active power without any response to AGC dispatch requirement. The P_{OUT} of the unit no longer follows the input signal P_{SET}. Therefore, those historical operation data under the off-regulation mode must be eliminated in advance because it is not useful to evaluate the AGC dynamic performance.

Second, in Fig. 4, the error tolerance band of the P_{SET} is commonly called the dead-band. Frequently, a real-time updated step of the P_{SET} may fail to cross the current dead-band. The dispatch order cannot trigger an effective response of the AGC unit. Apparently, for an accurate evaluation, the effect of dead-band on P_{SET} must also be eliminated by dead-band checking.

Generally, the value of dead-band is a percentage of P_{SET} or a certain value (e.g. Germany is ±5%P_{SET} and China is ±2MW). As an illustration in Fig. 5, dead-band is assumed to be 2MW. P'_{SET} is the dead-band checked signal. At times t_1, t_2, and t_3, the P_{SET} is updated. Whenever the amplitude of the new step is less than 2MW, P'_{SET} remains the same as the previous step. In this paper, all the input signal P_{SET} mentioned below are filtered by dead-band checking, which avoids the influence of frequent small-span P_{SET} on AGC performance analysis.

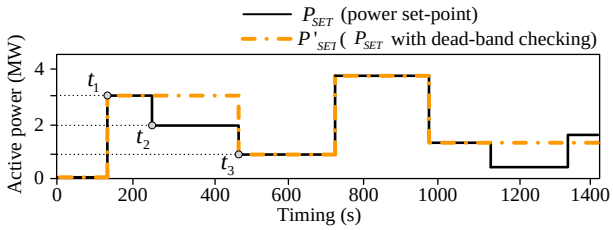

Fig. 5. Dead-band checking with 2MW error tolerance for P_{SET}.

Third, power system frequency control includes primary frequency control and secondary frequency control. The former is mainly determined by the governor itself, the latter is relied on the AGC unit. For the common, the process of primary frequency control to recover frequency stability is often within 30s[41]. When the frequency deviation of the power grid exceeds the maximum capacity of primary frequency control, the AGC unit adjusts the output according to P_{SET} to restore a wider range of frequency deviation. Compared with the secondary frequency response, the fluctuation of the primary frequency response is with short time scale and the amplitude is smaller. It is necessary to eliminate the influence of primary frequency control on P_{OUT} by using a low-pass noise filter. In this paper, the Savitzky Golay filter[34] is used because it preserves the shape and width of the original signal, and there is no lag in the filtered data.

As shown in Fig. 6, the solid blue line P'_{OUT} is the filtered signal. Small amplitude and high frequency noise in P_{OUT} is well removed by the filter. From now on, all P_{OUT} mentioned below are pre-filtered to avoid the effects of the primary frequency control, highlighting the characteristics of the secondary frequency response based on AGC.

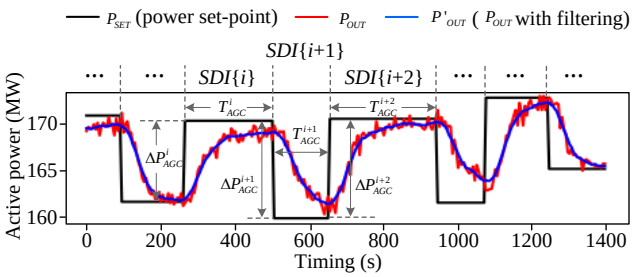

Fig. 6. Primary response filtering for P_{OUT} and segmentation of single dynamic interval.

3.2. Construction of AGC sample space

Features of AGC-related performance are retained after data preprocessing. In order to obtain a further refined evaluation, a concept of "AGC sample space" is proposed. A single AGC sample is defined as follows.

For an AGC unit, the range from receiving a P_{SET} step to receiving the next P_{SET} step is named a Single Dynamic Interval (*SDI*). Apparently, in a *SDI*, the dynamic performance mainly depends on two factors, that is, the duration of the step (T_{AGC}) and the amplitude of the step (ΔP_{AGC}). The ΔP_{AGC} is defined relative to the previous step and assumed to be positive for increasing and negative for decreasing.

As shown in Fig 6, the historical data of AGC is divided into several independent SDI. Each SDI is a single AGC sample, in which the performance of P_{OUT} is different. As defined by Eq(2), the product of T_{AGC} and ΔP_{AGC} is called S_{SET}, which equals to the desired regulation energy. S_{SET} is a rectangular area with positive or negative label, and other detailed definitions for regulation energy are as follows.

As shown in Fig 7, at time t_1, the output of the AGC unit is P_1. The unit receives a new P_{SET} step with T_{AGC} and ΔP_{AGC}, where $T_{AGC}=t_K-t_1$ (K is the number of sampling points in T_{AGC}). S_{Re} is the reverse regulation energy to P_1, and S_{Ex} is the expected regulation energy. The actual regulated energy of the AGC unit is defined by Eq (3) and Eq (4):

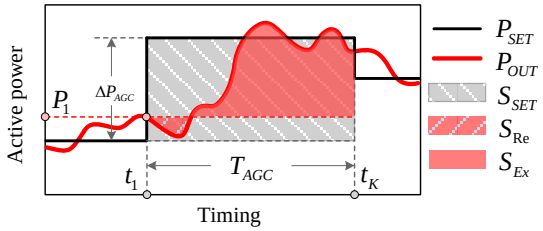

Fig. 7. Calculation of the desired and actual regulation energy in a single AGC sample.

$$S_{SET} = T_{AGC} \times \Delta_{AGC} \tag{2}$$

$$S_{OUT} = S_{Re} + S_{Ex} \tag{3}$$

$$\begin{cases} S_{Re} = \sum_{1}^{K} P_{OUT}(i) - P_1, & P_{OUT}(i) < P_1 \\ S_{Ex} = \sum_{1}^{K} P_{OUT}(i) - P_1, & P_{OUT}(i) > P_1 \end{cases} \tag{4}$$

Therefore, the cumulative tracking error between P_{OUT} and P_{SET} of the AGC unit can be defined by Eq (5):

$$E_{SDI} = \left| S_{SET} - S_{OUT} \right| \tag{5}$$

E_{SDI} describes the tracking performance in each *SDI* as the difference between the actual regulated energy and the desired regulation energy.

Thus, each AGC sample contains three different features, namely T_{AGC}, ΔP_{AGC}, and E_{SDI}. All samples are mapped into a three-dimensional space, forming an AGC sample space *V*.

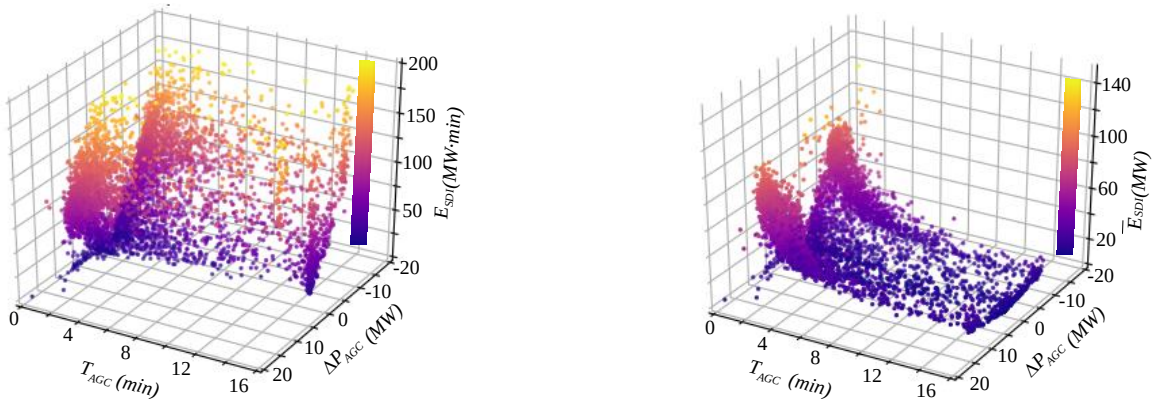

(a) (b)

Fig. 8. Data distribution of AGC samples in a three-dimensional space *V*: (a) AGC samples with T_{AGC}, ΔP_{AGC} and E_{SDI}, (b). AGC samples with T_{AGC}, ΔP_{AGC} and $\bar{E}_{SDI}$ (standardized by T_{AGC}).

Taking a real AGC unit from a power grid as an example, the AGC sample space within 30 days is shown in Fig 8 (the original data are from Power Utility). The *X*, *Y*, and *Z* axes of the sample space represent the duration $T_{AGC}(min)$, the amplitude $\Delta P_{AGC}(MW)$, and the cumulative tracking error $E_{SDI}(MW \cdot min)$, respectively. However, the distribution of the samples is chaotic and has no significant regularity. Considering that E_{SDI} is the cumulative tracking error, the value of E_{SDI} is affected by the cumulative time T_{AGC}. As a consequence, E_{SDI} must be standardized by Eq(6):

$$\bar{E}_{SDI} = E_{SDI} / T_{AGC} \tag{6}$$

$\bar{E}_{SDI}$ describes the average tracking error of an AGC sample, as shown in Fig 8(b), the distribution of the samples exhibits

clear boundaries and regularities. It can be seen that $\bar{E}_{SDI}$ gradually decreases with increasing T_{AGC}, and gradually increased with the increase of the absolute value of ΔP_{AGC}. The reason is that a larger T_{AGC} means that the output of the unit will gradually stabilize during the regulation process. On the other hand, a larger ΔP_{AGC} means that the power grid expects a larger power regulation range for the AGC unit, which is relatively difficult.

The AGC-related data preprocessing highlights the characteristics of the sample space. As shown in Fig 9(a), after removing the off-regulation mode data, the AGC samples formed two distinct clusters around ΔP_{AGC}=±10 MW, indicating a higher probability for an AGC unit to receive such regulation order during its daily operation. In addition, it can be seen from the Fig 9(b) that after dead-band checking and primary frequency filtering, samples with the absolute value of ΔP_{AGC}<2MW and a small number of outliers are eliminated.

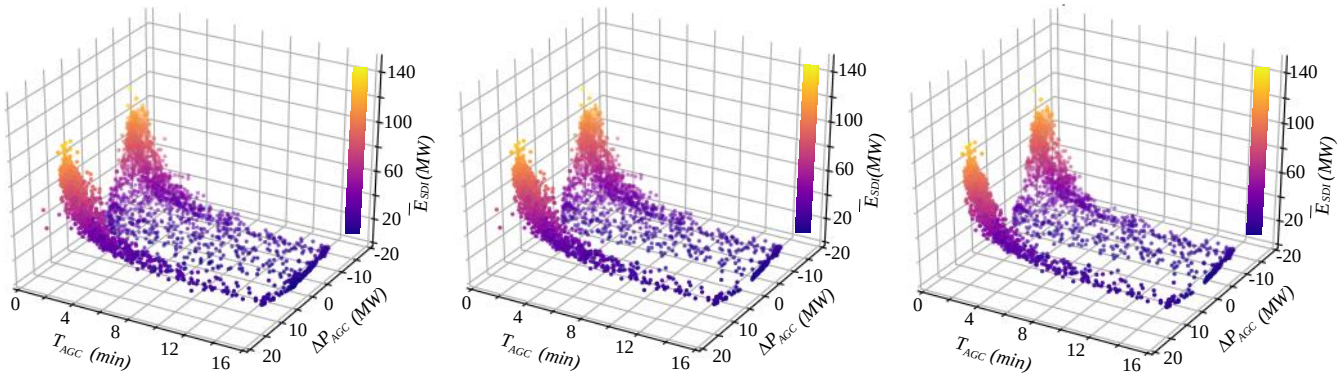

(a) (b) (c)

Fig. 9. Data distribution changes after data preprocessing and data cleaning: (a). Sample space after removing the off-regulation mode data, (b). Sample space after dead-band checking and primary frequency filtering, (c). Sample space after data cleaning.

Furthermore, there are still some outliers in the sample space after data preprocessing, which may interfere with the performance evaluation. To this end, a data cleaning method based on local density is proposed.

Assuming that $V=\{Xi\}_{i=1}^{N}$, X_i=[$T_{AGC}(i)$, ΔP_{AGC} (i), $\bar{E}_{SDI}(i)$] represents each AGC sample and N is the total number of samples. d_{ij} means the distance between X_i and X_j, where $i,j \in \{1,2,\ldots,N\}$. In this study, d_{ij} is calculated according to the Euclidean Metric, which means that the d_{ij} between X_i and X_j is

$$d_{ij}=\sqrt{[T_{AGC}(i)-T_{AGC}(j)]^2+[\Delta_{AGC}(i)-\Delta_{AGC}(j)]^2+[\bar{E}_{SDI}(i)-\bar{E}_{SDI}(j)]^2} \quad (6)$$

For any X_i in the sample space V, the local density ρ_i is defined by Eq(7):

$$\rho_i=\sum_{i,j\in\{1,2,\cdots N\}} f(d_{ij}-d_c) \quad (7)$$

where $f(x)$=1 if x <0 and $f(x)$=0 otherwise, and d_c is a cutoff distance (d_c >0). Basically, ρ_i is equal to the number of neighbors that are closer than d_c to the X_i. The local density ρ_i is only sensitive to the relative magnitudes of different samples, which means that for large datasets, the analytical results are robust to the choice of d_c. Reference [42] pointed out that one can choose d_c so that the average number of neighbors is around 1% to 2% of the total number of samples in the dataset.

In this paper, d_c is selected by a percentage of 1.5%. Considering that N is the number of AGC samples, so the number of d_c is $M=N(N-1)/2$ and $d_1 \leqslant d_2 \leqslant \ldots \leqslant d_M$ is the ascending order of d_c. Let $d_c=d_q$ where q=<1.5%M>, and < >stands for rounding down. In order to achieve the desired cleaning effect, the cleaning threshold is set to 0.1max{ρ_1, ρ_2,…ρ_N}. The sample space after data cleaning is shown in Fig 9(c), where outliers with low local density are successfully removed.

Benefiting from data preprocessing and cleaning, the boundaries of AGC samples are gradually clear, which helps the dispatch center to analyze the performance of the unit with different T_{AGC} and ΔP_{AGC}.

3.3. *Multi-dimensional feature analysis of AGC sample space*

In the daily operation of the power grid, it is essential for the dispatch center to confirm the time it takes for a AGC unit to achieve its best tracking effect after receiving instructions. Verification by real engineering experiments is obviously unrealistic, as a consequence, a multi-dimensional feature analysis method based on data mining is proposed.

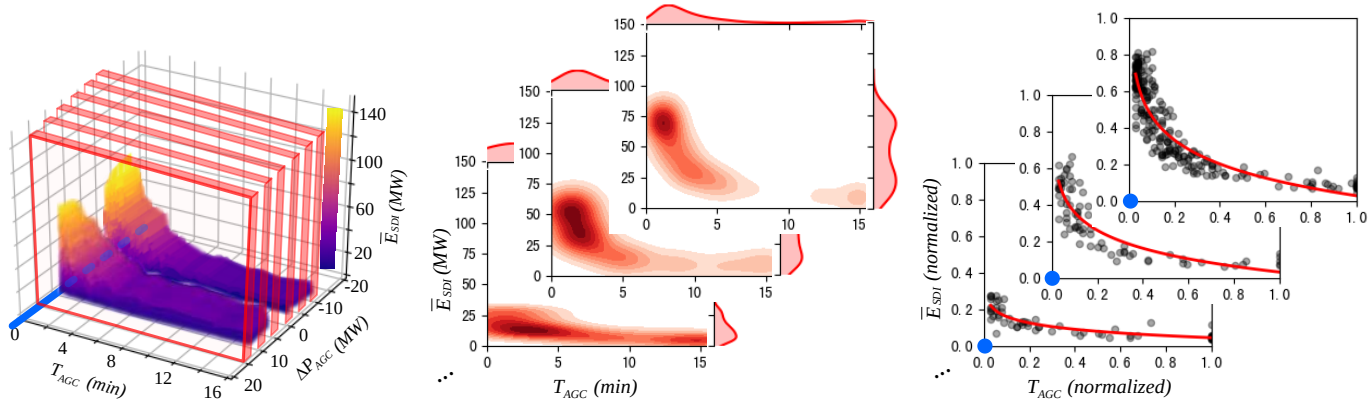

(a) (b) (c)

Fig. 10. Visualization of cutoff intervals of AGC sample space: (a). Successive segmentation of AGC samples along the axis of ΔP_{AGC}, (b). AGC sample distribution densities in different cutoff intervals, (c). Fitting curves of AGC samples in different cutoff intervals.

As shown in Fig 10(a), for visual illustration, clusters of AGC samples might as well to be visualized as data blocks, which are then segmented by successive cutoff intervals along the ΔP_{AGC} axis. If the thickness of each cutoff interval is δ, then the number of intervals is $(max\Delta P_{AGC}\text{-}min\Delta P_{AGC})/\delta$.

As shown in Fig 10(b), AGC samples show different distribution characteristics in different cutoffs. The shade darkness in each subplot of Fig 10(b) reflects the density of the samples. The curves on the axes are probability density curves, which independently reflect the probability distribution of T_{AGC} and $\bar{E}_{SDI}$, respectively. Intuitively, each subplot presents a darkest shade center. However, the shade center only indicates that the AGC unit has a higher probability of receiving such power setpoint and does not imply optimal performance.

For an accurate evaluation, scatter points in each cutoff interval are mapped to a two-dimensional plane. It is assumed here that the coordinates of scatter points $(x,y)=(T_{AGC(i)}, \bar{E}_{SDI(i)})$ satisfy a higher-order polynomial defined by Eq(8), and the objective function is defined by Eq(9).

$$y = g(x) = a_0 + a_1 x + a_2 x^2 + \cdots + a_k x^k \tag{8}$$

$$\begin{aligned} Loss &= \sum_{i=1}^{n} (\bar{E}_{SDI(i)} - y_{(i)})^2 \\ &= \sum_{i=1}^{n} \left[\bar{E}_{SDI(i)} - (a_0 + a_1 x_{(i)} + a_2 x_{(i)}^2 + \cdots + a_k x_{(i)}^k) \right]^2 \end{aligned} \tag{9}$$

where $\bar{E}_{SDI(i)}$ is the true values and $y_{(i)}$ is the polynomial fitting values. The ideal fitting curve is obtained by minimizing Eq(9), that is, making the partial derivative of each coefficient in Eq(9) equal to 0:

$$\frac{\partial Loss}{\partial a_0} = \frac{\partial Loss}{\partial a_1} = \cdots = \frac{\partial Loss}{\partial a_k} = 0 \tag{10}$$

Each coefficient in Eq(8) is obtained by Eq(10). Nonlinear fitting curves are shown in Fig 10(c). The fitting curve represents the regularity of the tracking error of the unit in different ΔP_{AGC} cutoff interval.

Assuming an AGC unit is absolutely perfect, this unit will drop $\bar{E}_{SDI}$ to zero without delay, regardless of the ΔP_{AGC} it receives. It indicates that all AGC samples of this unit will be distributed on the axis of $\bar{E}_{SDI}$=0 and T_{AGC}=0, which is shown by the blue line in Fig 10(a) and blue points in Fig 10(c). It can be considered as the "perfect performance axis" and the "perfect performance points".

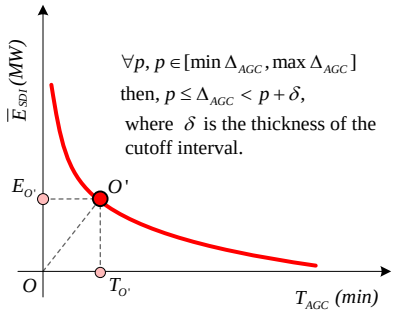

(a)

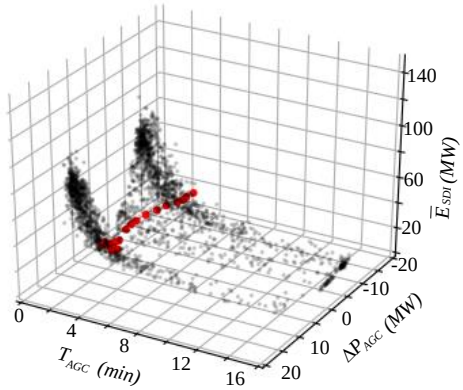

(b)

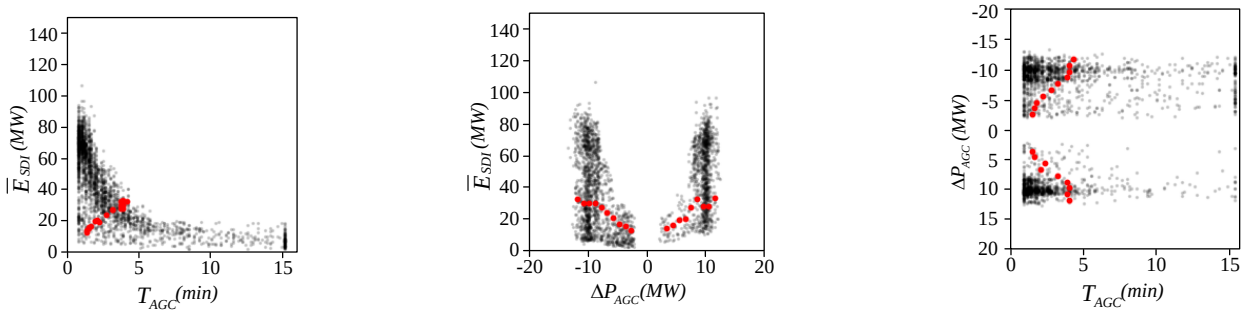

Fig. 11. Calculation principle and visualization of optimal performance points O': (a). The calculation of O' in a single cutoff interval, (b). Distribution of O' over all cutoff intervals in sample space, (c). Distribution of O' in the "T_{AGC}-$\bar{E}_{SDI}$" plane, (d). Distribution of O' in the "ΔP_{AGC}-$\bar{E}_{SDI}$" plane, (e). Distribution of O' in the "T_{AGC}-ΔP_{AGC}" plane.

As shown in Fig 11(a), in the two-dimensional plane of each cut-off interval, the point on the fitting curve closest to the origin O is $O'(T_{O'}, E_{O'})$, which is called the optimal performance point, that is, the unit output is closest to perfect. $T_{O'}$ represents the time required for the unit to achieve optimal performance, and the length of the line segment OO' is $d_{OO'} = \sqrt{T_{O'}^2 + E_{O'}^2}$ quantifying the deviation between optimal and perfect performance, called "coefficient of performance deviation".

Analyzing the $\bar{E}_{SDI}$-axis in Fig 11(a), there are still many points on the fitting curve that are lower than $E_{O'}$, just with higher T_{AGC} values. However, from the AGC control purpose of the power grid, the frequency gap of the grid must be restored as quickly as possible. The optimal performance point O' refers to the point where the tracking error reaches a lower level in the shortest time. The physical meaning of $O'(T_{O'}, E_{O'})$ in actual engineering is that when $p \leqslant \Delta P_{AGC} \leqslant p+\delta\ (\forall p,\ p \in [\min \Delta P_{AGC}, \max \Delta P_{AGC}])$, it takes $T_{O'}$ minutes for an AGC unit to realize the optimum output for itself, with the tracking error $d_{OO'}$.

For an AGC unit, the three-dimensional distribution of O' in a sample space is shown in Fig 11(b) and the projections in different directions are shown from Fig 11(c) to (e) respectively. It can be seen from Fig 11(d) that when the absolute value of ΔP_{AGC} increases, the $\bar{E}_{SDI}$ of O' shows an increasing trend. Similarly, in Fig 11(e), the T_{AGC} values of O' also increases with the absolute value of ΔP_{AGC}. Apparently, this is because the higher the absolute value of ΔP_{AGC}, the more difficult the AGC regulation task is, and the more time-consuming and error it takes to achieve optimal performance. Other detailed results are presented in Section 4.1.

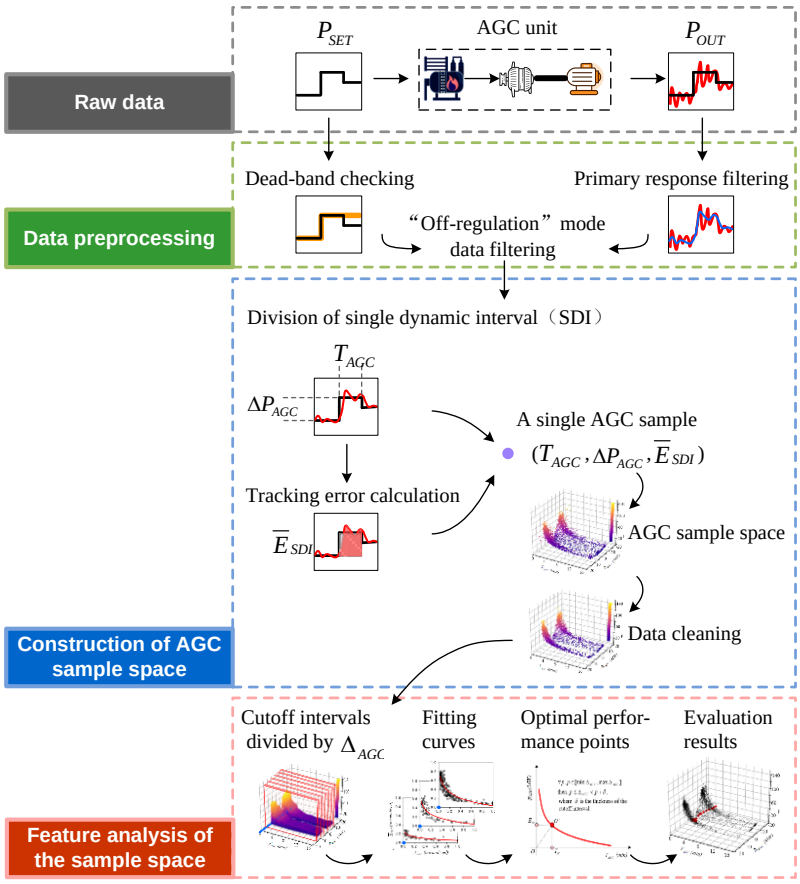

Fig. 12. Schematic diagram of the proposed AGC performance evaluation method.

In the sum, optimal performance evaluation of the AGC units is based on multi-dimensional feature and the overall schematic diagram is shown in Fig 12. In the following, the proposed method is verified based on real data of multiple AGC units.

4. Experiment results and analysis

The experimental data used in this paper come from eight thermal AGC units in a provincial-level regional power grid in China. Including the actual active power output of each AGC unit and the power set-point sent from the dispatch center. The sampling interval is 5 seconds. The time span of historical data is one month (30 days in total).

4.1. Optimal dynamic performance evaluation results

According to the proposed AGC performance evaluation method, the optimal performance evaluation results for different units within different set-point power are shown in Table I. In the first row of Table I, the letters A~H represent the names of the eight AGC units used in the experiment. The first column of the table is the cut-off interval of the set-point power ΔP_{AGC} received by the unit. In the second row of Table I, $T_{O'}$ and $d_{OO'}$ are two parameters of the optimal dynamic performance point O', where $T_{O'}$ is the time required for the unit to achieve optimal performance, and $d_{OO'}$ is the corresponding tracking error. The 'N' in the table represents that there are not enough AGC samples in the corresponding ΔP_{AGC} cutoff interval to form the optimal performance point.

TABLE I
Optimal performance points O' evaluation results accompanied by $T_{O'}$ and $d_{OO'}$ for different AGC units within different ΔP_{AGC}.

ΔP_{AGC} (MW)	A (350MW)		B (330MW)		C (300MW)		D (300MW)		E (300MW)		F (300MW)		G (200MW)		H (330MW)	
	$T_{O'}$ /min	$d_{OO'}$	$T_{O'}$ /min	$d_{OO'}$	$T_{O'}$ /min	$d_{OO'}$	$T_{O'}$ /min	$d_{OO'}$	$T_{O'}$ /min	$d_{OO'}$	$T_{O'}$ /min	$d_{OO'}$	$T_{O'}$ /min	$d_{OO'}$	$T_{O'}$ /min	$d_{OO'}$
[-19,-18]	N	N	N	N	N	N	N	N	N	N	4.70	68.89	N	N	N	N
[-18,-17]	N	N	N	N	N	N	N	N	N	N	4.40	71.89	N	N	1.96	106.38
[-17,-16]	N	N	N	N	N	N	N	N	N	N	N	N	N	N	N	N
[-16,-15]	N	N	N	N	N	N	N	N	N	N	N	N	4.03	83.66	N	N
[-15,-14]	N	N	N	N	N	N	N	N	N	N	N	N	5.24	69.05	N	N
[-14,-13]	N	N	N	N	N	N	N	N	N	N	N	N	5.55	49.83	N	N

[-13,-12]	N	N	N	N	3.22	25.75	3.97	16.36	N	N	4.26	57.53	4.33	62.03	3.30	70.18
[-12,-11]	4.25	15.09	3.40	19.57	3.37	16.51	3.69	18.77	3.40	18.83	3.83	28.17	4.49	48.80	4.04	49.14
[-11,-10]	3.97	14.13	3.40	18.53	3.22	17.53	3.69	18.15	3.12	24.39	3.69	23.52	3.73	50.90	3.30	50.09
[-10,-9]	3.97	14.02	3.26	17.86	3.07	17.10	3.55	18.22	3.40	23.57	3.55	23.49	N	N	1.67	80.22
[-9,-8]	3.83	13.64	3.40	21.24	3.22	21.71	3.40	21.33	3.83	24.08	3.26	31.12	N	N	1.22	77.23
[-8,-7]	3.26	13.61	2.70	15.62	2.33	21.57	2.70	30.40	3.26	27.50	1.85	53.25	N	N	N	N
[-7,-6]	2.84	12.83	2.13	16.82	2.19	15.96	2.70	19.24	2.98	24.54	N	N	N	N	N	N
[-6,-5]	2.27	12.48	1.85	15.12	1.59	14.54	1.85	22.39	2.27	24.77	N	N	2.36	57.51	N	N
[-5,-4]	1.85	11.22	1.42	13.94	1.15	16.30	1.42	26.05	1.99	25.02	N	N	N	N	1.67	69.29
[-4,-3]	1.71	10.54	1.14	12.69	1.15	14.53	N	N	1.57	19.37	N	N	N	N	N	N
[-3,-2]	1.57	8.92	1.14	11.32	N	N	N	N	N	N	N	N	N	N	N	N
[2,3]	N	N	1.14	13.84	N	N	N	N	N	N	N	N	N	N	2.56	60.12
[3,4]	1.57	10.49	1.28	15.23	1.59	22.48	N	N	1.28	13.99	N	N	N	N	1.52	67.55
[4,5]	1.71	11.93	1.57	16.92	N	N	N	N	N	N	N	N	N	N	1.96	61.51
[5,6]	2.41	11.19	1.85	19.04	2.04	24.10	N	N	N	N	N	N	2.82	61.88	N	N
[6,7]	2.13	14.25	2.41	24.11	2.48	20.87	N	N	N	N	1.42	49.10	5.09	36.08	2.56	79.57
[7,8]	3.26	14.24	2.84	21.37	3.22	21.65	2.41	44.52	N	N	2.41	36.44	3.58	56.04	3.30	70.73
[8,9]	3.83	17.05	3.40	18.55	3.37	20.58	3.40	30.40	2.70	43.77	3.55	28.18	4.94	47.10	4.63	42.27
[9,10]	3.97	12.27	3.40	17.70	3.37	17.84	3.55	25.93	2.98	33.17	3.69	23.31	6.30	33.18	2.70	70.70
[10,11]	3.83	11.94	3.55	21.24	3.37	18.81	3.83	15.38	2.98	22.95	3.97	22.90	6.46	31.35	4.93	63.85
[11,12]	3.97	16.56	3.12	23.82	3.22	23.10	4.11	14.87	3.26	23.14	3.97	26.39	6.76	29.07	4.63	52.24
[12,13]	N	N	N	N	3.07	30.16	N	N	3.55	23.41	4.40	36.38	6.61	35.78	6.26	28.86
[13,14]	N	N	N	N	N	N	N	N	3.69	29.53	4.57	66.21	6.76	37.67	N	N
[14,15]	N	N	N	N	N	N	N	N	N	N	4.97	41.52	6.76	37.90	N	N
[15,16]	N	N	N	N	N	N	N	N	N	N	N	N	6.91	39.26	N	N
[16,17]	N	N	N	N	N	N	N	N	N	N	N	N	6.46	53.48	N	N
AVE	**2.96**	**12.97**	**2.42**	**17.73**	**2.61**	**19.74**	**3.10**	**23.51**	**2.89**	**25.13**	**3.51**	**35.00**	**5.33**	**43.73**	**3.13**	**61.56**

For T_O, columns in Table I, taking unit-A as a typical example, the value of T_O, shows a gradually increasing trend as the absolute value of ΔP_{AGC} increases. Apparently, it means that the task received by the AGC unit is more difficult, and it takes a longer time to reach the optimal performance point. Although there are some individual values of T_O, from other unit that do not strictly satisfy this regularity, the trend is still clear under the data-driven analysis.

For $d_{OO'}$ columns in Table I, taking unit-F as a typical example, when ΔP_{AGC}<0, the tracking error $d_{OO'}$ reaches the minimum 23.49 where ΔP_{AGC}=[-10MW,-9MW]. Conversely, when ΔP_{AGC}>0, the tracking error $d_{OO'}$ reaches the minimum 22.90 where ΔP_{AGC}=[10MW,11MW]. It indicates that unit-F is good at different ΔP_{AGC} intervals when adjusting its output power.

For ΔP_{AGC} rows in Table I, taking ΔP_{AGC}=[-11MW,-10MW] as a typical example, the T_O, of unit-E is the lowest (3.12min), indicating that unit-E takes the shortest time to achieve optimal performance among all units. Correspondingly, the $d_{OO'}$ of unit-A is the lowest (14.13), indicating that the tracking accuracy of unit-A is the best among all units.

Table I reflects the different performance characteristics of single or multiple AGC units, and the proposed evaluation method is verified as follows.

4.2. *Verification of the proposed evaluation method on AGC units*

For AGC units, the rationality of the optimal performance evaluation needs to be verified. Here, a strict evaluation metric named $K_P^{i,j}$ is used as the verification method, as defined by Eq(11). The $K_P^{i,j}$ metric is also called "*K*-method".

$$K_P^{i,j} = K_{1\_NF}^{i,j} \times K_{2\_NF}^{i,j} \times K_{3\_NF}^{i,j} \tag{11}$$

$K_P^{i,j}$ is the comprehensive performance for the *j* th independent response of the *i* th AGC unit. According to the definition in the "*K*-method" regulation, $K_{1\_NF}^{i,j}=K_1^{i,j}/v_i$, where $K_1^{i,j}$ is the actual regulation speed and v_i is the standard regulation speed of the unit. $K_{2\_NF}^{i,j}=2-K_2^{i,j}/(T_{i,j}*s_i)$, where $K_2^{i,j}$ is the actual regulation deviation, $T_{i,j}$ is the duration of the deviation and s_i is the permitted deviation of the unit. $K_{3\_NF}^{i,j}=2-K_3^{i,j}/t_i$, where $K_3^{i,j}$ is the actual response delay and t_i is the standard response delay. The calculation of $K_1^{i,j}$, $K_2^{i,j}$, and $K_{3\_}^{i,j}$ is shown in Fig 4(b) in Section II. After normalization, the higher the value of $K_P^{i,j}$, the better the comprehensive performance of AGC units.

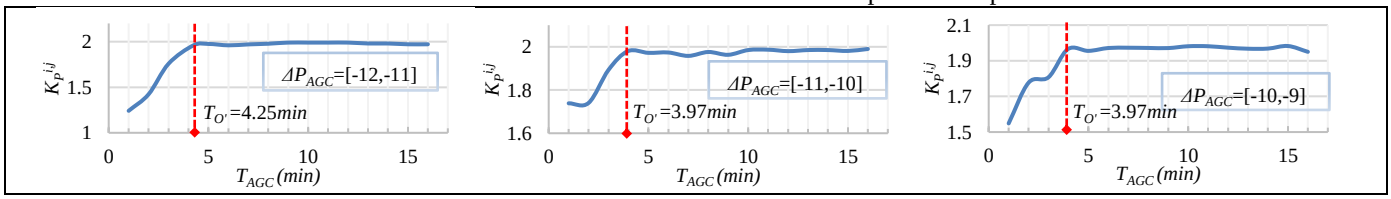

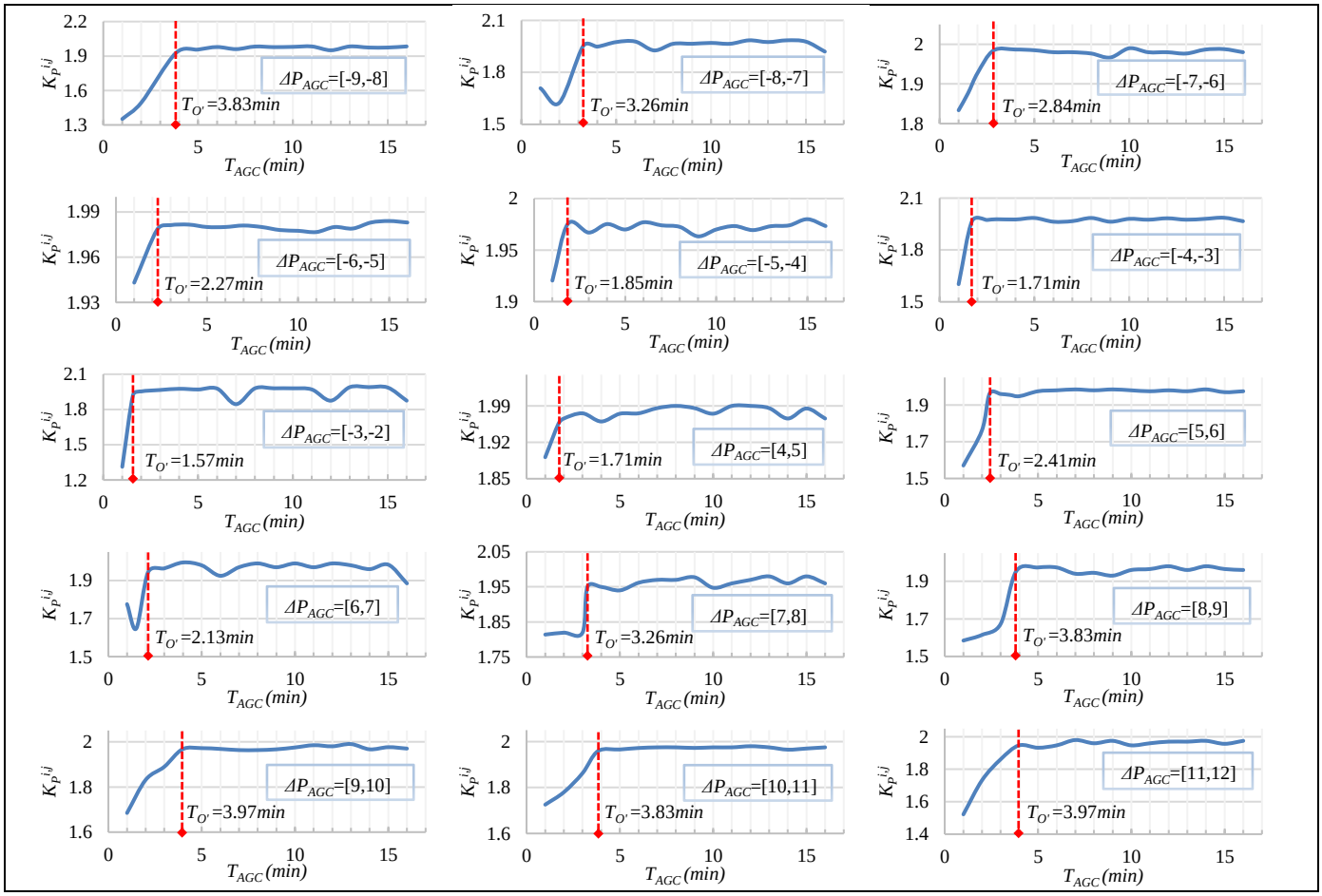

Fig. 13. Comparison between K_P curves (blue line) from K-method and $T_{O'}$ (red line) from proposed method in different ΔP_{AGC} intervals.

Taking unit-A as a typical example, the $K_P^{i,j}$ curves (blue lines) are shown in Fig 13, where the red dotted lines represent the location of $T_{O'}$. Each subfigure of Fig 13 is generated from different ΔP_{AGC} intervals. With the increase of T_{AGC}, the blue K_P curve reaches its peak at $T_{O'}$ and tends to be stable. It means that AGC unit begin to achieve the optimal comprehensive performance at $T_{O'}$. In other words, the optimal performance points obtained by the proposed method is consistent with the K-method.

In addition, it is a practical requirement for the dispatching center to compare the performance of different AGC units. Therefore, it is necessary to verify the performance ranking of different AGC units for the proposed method. In K-method, $\bar{K}_P^{i,j}$ is the average of $K_P^{i,j}$ for each AGC unit, which represents the overall performance in a period of time. In the proposed method, $\bar{d}_{OO'}$ is the average of $d_{OO'}$, which describes the gap between optimal performance and perfect performance, and $\bar{d}_{OO'}$ also quantifies the overall performance of each unit. The difference is that the better the performance of the unit, the higher the $\bar{K}_P^{i,j}$, and the lower the $\bar{d}_{OO'}$. $\bar{K}_P^{i,j}$ and $\bar{d}_{OO'}$ of different AGC units are shown in Table II. It can be seen from the Table II that in the ranking results of multiple AGC units, $\bar{K}_P^{i,j}$ and $\bar{d}_{OO'}$ show opposite trends. It means that the proposed method and the conventional method provide consistent overall ranking results of the comprehensive performance.

TABLE II
Ranking results of $\bar{K}_P^{i,j}$ and $\bar{d}_{OO'}$ of multiple AGC units

	A (350MW)	B (330MW)	C (300MW)	D (300MW)	E (300MW)	F (300MW)	G (200MW)	H (330MW)
$\bar{K}_P^{i,j}$	3.587	2.376	2.147	1.601	1.364	0.562	0.125	0.029
$\bar{d}_{OO'}$	12.97	17.73	19.74	23.51	25.13	35.00	43.73	61.56

It should be emphasized that the proposed method can provide more detailed information. Data of $d_{OO'}$ in Table I can be visualized by a three-dimensional histogram shown in Fig 14. It accurately disperses the $d_{OO'}$ into independent intervals. The horizontal axis of the histogram is ΔP_{AGC}, and the longitudinal axis is $d_{OO'}$. It can be seen that when the overall performance of AGC units is better, the distribution of $d_{OO'}$ tends to be lower and more stable. Furthermore, when ΔP_{AGC} in Fig 14 belongs to

a certain interval, the performance ranking of AGC units may change.

Taking unit-D as an example, when 10MW≤ΔP_{AGC}≤12MW, the $d_{OO'}$ of unit-D is about 14 to 15 (the value can be checked in Table I), reaching a relatively low level. For the dispatch center, it means that when 10MW≤ΔP_{AGC}≤12MW, unit-D can be used as a target unit with higher priority. On the other hand, for unit-D itself, it also can be seen in Fig 14 that the overall level of $d_{OO'}$ is lower and more stable when ΔP_{AGC} <0. It means that in the daily operation of unit-D, the overall performance of reducing power is often better than that of increasing power.

Taking unit-F as another example, it can be seen in Fig 14 that although the histogram of $d_{OO'}$ has several peaks, when -11MW≤ΔP_{AGC}≤-9MW or 9MW≤ΔP_{AGC}≤11MW, $d_{OO'}$ still reaches a low level. To some extent, it indicates that even the comprehensive performance of unit-F is not outstanding, it is still good at executing AGC instructions with specific amplitude. On the other hand, it indicates that some undesirable performances of AGC units are actually caused by the instructions from the dispatch center. In the sum, the difficulty of AGC tasks undertaken by different AGC units is accurately distinguished by the proposed method.

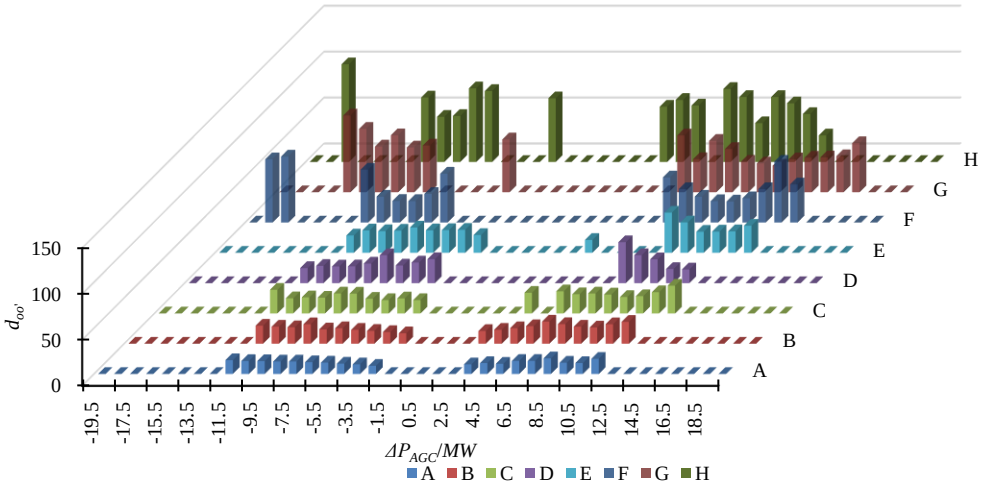

Fig. 14. Three-dimensional histogram of $d_{OO'}$ of different AGC units in different ΔP_{AGC} intervals.

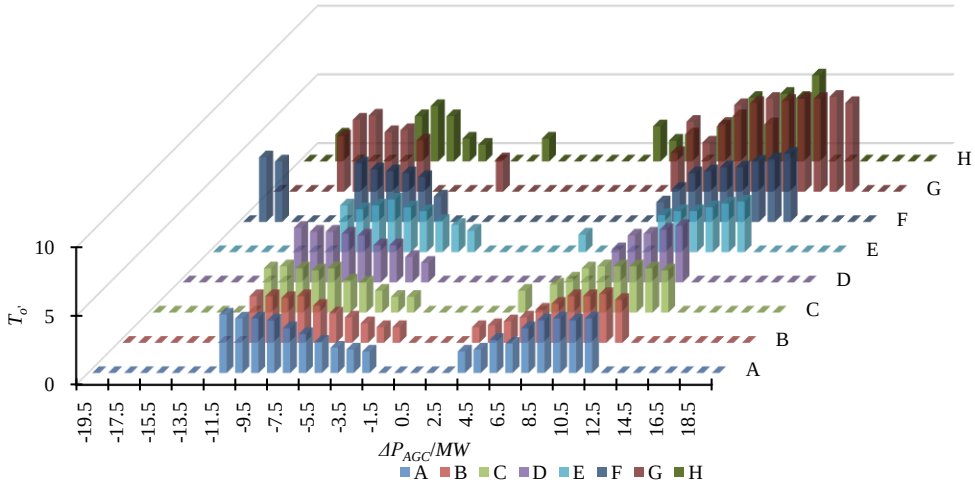

Fig. 15 Three-dimensional histogram of $T_{O'}$ of different AGC units in different ΔP_{AGC} intervals.

Furthermore, another indicator $T_{O'}$ can also be dispersed into independent intervals. $T_{O'}$ means the time taken by the AGC unit to achieve its optimal performance, and the visualization of $T_{O'}$ is shown in Fig 15. From the distribution of the histogram, the $T_{O'}$ of each unit shows an upward trend with the increase of the absolute value of ΔP_{AGC}. The mean $T_{O'}$ of unit-B reached the minimum value 2.42min (the value can be checked in Table I), while that of unit-G reached the maximum value 5.33min. It is worth noting that when -6MW≤ΔP_{AGC}≤-5MW or 5MW≤ΔP_{AGC}≤6MW, the $T_{O'}$ of unit-G still reaches a relatively low level. It indicates that although the comprehensive performance of unit-G is not excellent, unit-G still good at executing AGC instructions with amplitude between 5MW and 6MW. Furthermore, it can be seen that unit-F and unit-G often undertake the

difficult AGC tasks such as ΔP_{AGC}<-13MW and ΔP_{AGC}>14MW.

According to the above analysis, compared with the single index of conventional methods, the proposed method provides multi-dimensional index of AGC performance based on data-driven. The instructions that AGC units are good at can be obtained, and the time consumption and tracking error for AGC units to achieve their own optimal performance are given in detail. In other words, when the dispatch center selects the available AGC units and the value of ΔP_{AGC}, the decision-making is diversified enough to adapt to different secondary frequency control tasks of the power grid.

4.3. *Verification of the advantage of the proposed method*

Different set-point power with different ΔP_{AGC} and T_{AGC} are considered in the proposed method. As for the analysis of conventional AGC evaluation systems in Section II, *K*-method is the strictest evaluation method. In fact, in the *K*-method, AGC samples can also be distinguished by ΔP_{AGC} and T_{AGC}. Therefore, it is necessary to compare the *K*-method with the proposed method in the same time span.

Taking Unit-A as an example, the data distribution of regulation speed K_1, regulation deviation K_2 and response delay K_3 are shown in Fig 16. The comparison between the *K*-method and the proposed method is shown in Fig 17. As a data driven analysis, if the time span of historical data is too small, the regularity of AGC samples is not significant enough. In contrast, if the time span is too large, the characteristics of data distribution will be blurred. Therefore, the time span of Fig 16 and Fig 17 is set to 30 days to ensure that sufficient information is reflected.

According to Eq(11), $K_1 \in [0, +\infty]$, $K_2 \in [0,2]$ and $K_3 \in [0,2]$. The higher the values of K_1, K_2 and K_3, the better the performance of AGC units. It can be seen from Fig 16 that K_2 performs relatively well, which indicates that Unit-A has high regulation accuracy. However, no more detailed information can be obtained from the sample space. Neither K_1, K_2 nor K_3 has any valuable regularities in the dimensions of ΔP_{AGC} and T_{AGC}.

The comprehensive performance $K_P = K_1 * K_2 * K_3$ of *K*-method is shown in Fig 17(a), and $\bar{E}_{SDI}$ of the proposed method is shown in Fig 17(b). It can be seen that the AGC samples processed by the proposed method show significant regularity, which is also the basis for multi-dimensional feature analysis.

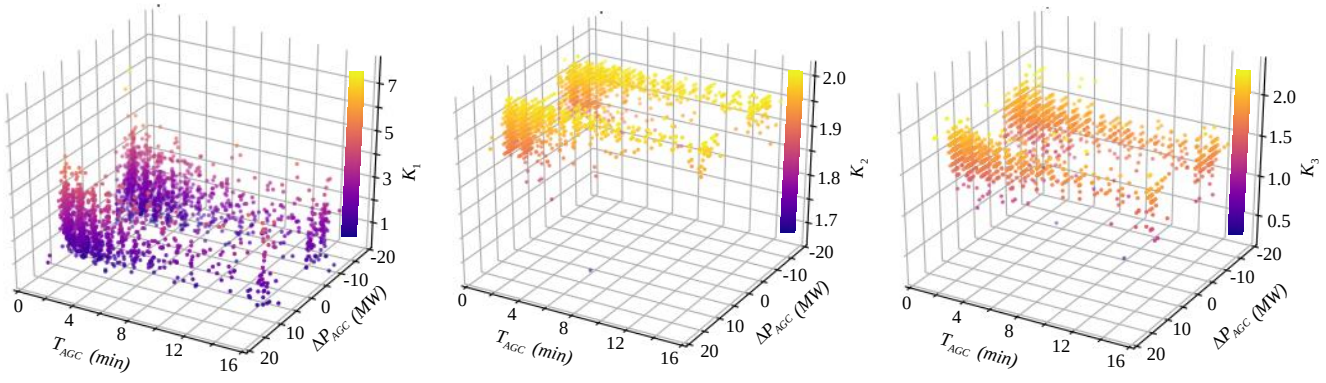

(a) (b) (c)

Fig. 16. Data distribution of *K*-method in AGC sample space: (a). AGC sample space of regulation speed K_1, (b). AGC sample space of regulation deviation K_2, (c). AGC sample space of response delay K_3.

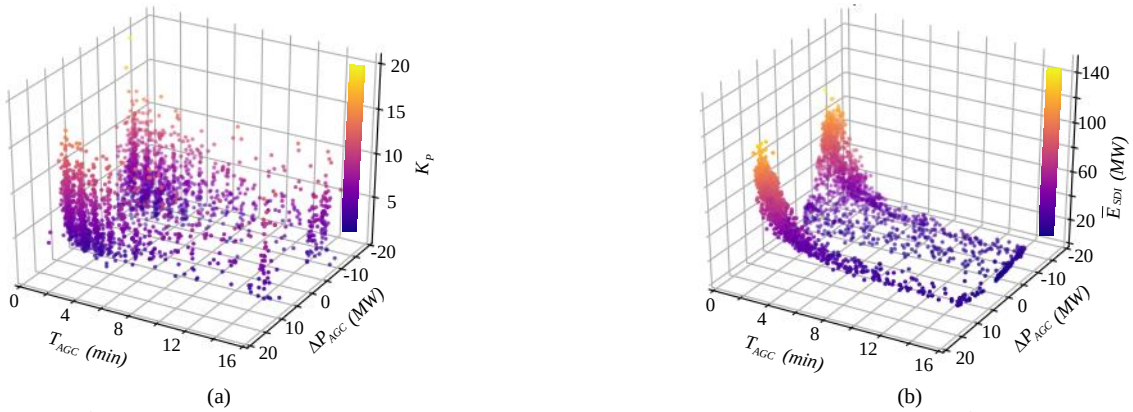

(a) (b)

Fig. 17. Comparison of data distribution between conventional *K*-method and the proposed method: (a). AGC sample space of comprehensive performance K_P, (b). AGC sample space of the proposed index $\bar{E}_{SDI}$

In addition, another practical advantage of the proposed method is that it solves the common problem of evaluation failures in *K*-method. The calculation of *K*-method depends on whether the output of AGC unit crosses the error tolerance boundary, which is usually called “dead-band”. Once the AGC unit fails to cross the dead-band, K_1, K_2 and K_3 cannot be obtained.

Some typical failure examples in *K*-method are illustrated in

Fig 18. In each subfigure, the black line is the set-point power P_{SET} sent from the dispatch center, the red curve is the output power P_{OUT} of the AGC unit, the yellow area is the dead-band (the dead-band boundary is ±2MW), and the range of each evaluation failure is marked by a light gray area.

Taking Unit-A-(a) in Fig 18 as a typical example, it can be seen that at the beginning of timing, the P_{SET} is about 264MW, so the dead-band is from 262MW to 266MW. At nearly 200s, P_{SET} is reduced to around 256MW, the dead-band is also reduced to 254MW to 258MW. Obviously, the P_{OUT} successfully crossed the first dead-band at about 300s but failed to enter the second dead-band until the P_{SET} was updated again. The time period marked by the gray area is a typical evaluation failure in *K*-method, the AGC performance evaluation cannot be obtained during this period. In this situation, the index K_P is set to zero, and the output of AGC unit is judged as failure response, which means that AGC unit will receive severe economic penalties.

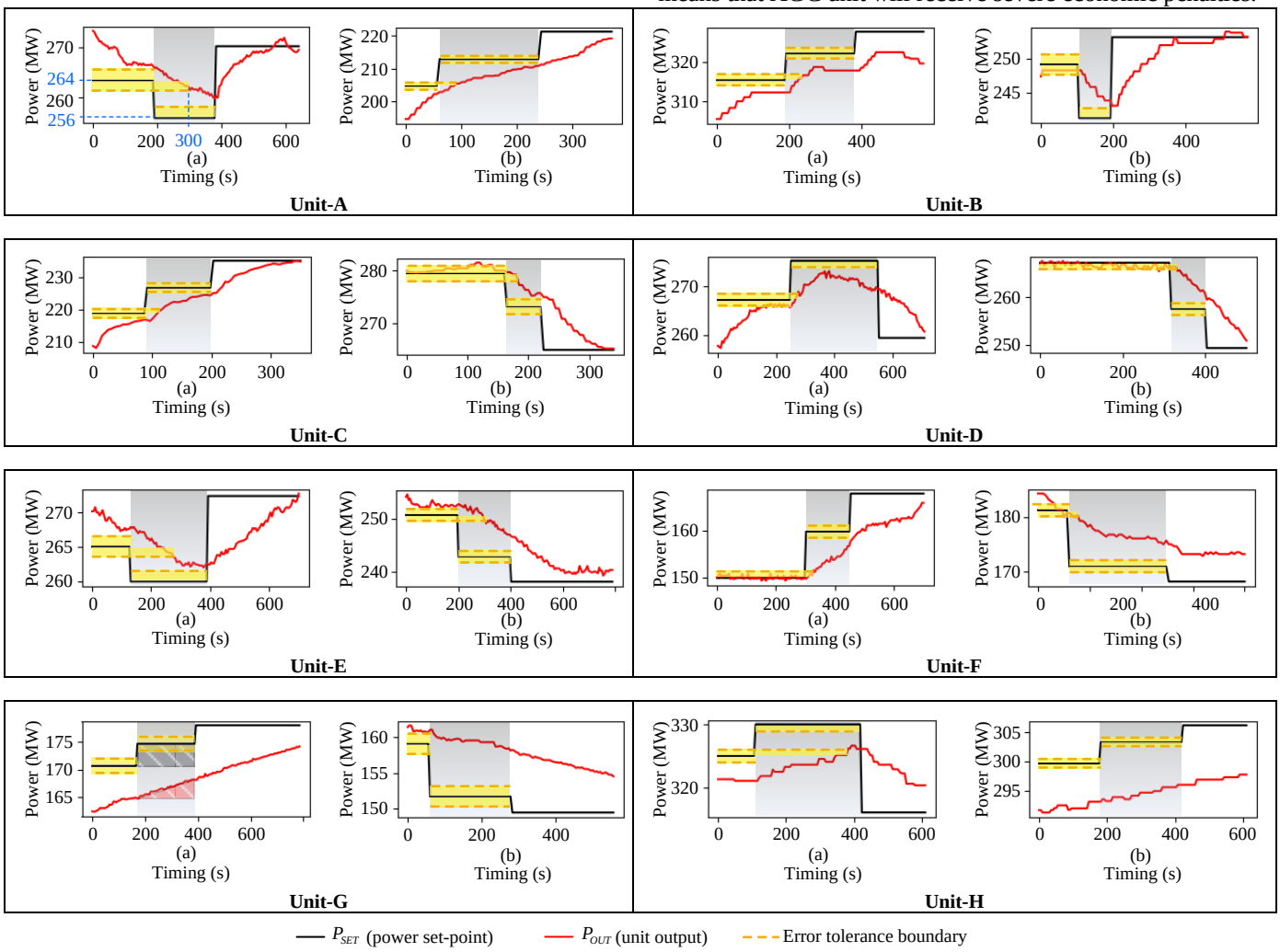

Fig. 18. Typical failure examples when AGC unit output failed to cross the dead-band under the conventional evaluation method.

However, this assessment is not completely fair for AGC units. In fact, in each gray area of Fig 18, it is clear that the P_{OUT} has actually made correct changes under the guidance of P_{SET}. Just because the P_{SET} has been changed before the P_{OUT} enters the target dead-band. That is to say, in conventional evaluation method, these so-called failure performances have actually made beneficial contributions to the power grid by adjusting their output. In the proposed method, the evaluation results are not affected by the dead-band. Taking Unit-G-(a) in Fig 18 as an example, the desired and the actual regulated energy calculated by the proposed method are shown by the gray and red areas with grids, respectively. As a result, the AGC performance is successfully quantified by the proposed method, which solving the evaluation failures in conventional method.

TABLE III
Statistics of evaluation failures under conventional evaluation method

Statistical items	Unit-A (350MW)	Unit-B (330MW)	Unit-C (300MW)	Unit-D (300MW)	Unit-E (300MW)	Unit-F (300MW)	Unit-G (200MW)	Unit-H (330MW)
Number of evaluation failures	511	868	1136	378	423	1503	1863	858
Number of total evaluations	1901	3324	3331	1122	1339	4612	7777	3037
Proportion of evaluation failures in total evaluations	26.88%	26.11%	34.10%	33.69%	31.59%	32.59%	23.96%	28.25%
Cumulative time of evaluation failures	31.68h	55.4h	55.52h	18.7h	22.32h	76.86h	129.62h	50.61h

Although expanding the width of the dead-band may alleviate the problem of evaluation failure to some extent, but it means that the requirements for AGC units are weakened, which inevitably affect the power quality of the energy system. The problem of evaluation failures usually occurs when AGC units are continuously required to increase or decrease their output, or when the output is required to reverse, which is very common in the daily operation of the energy system. Table III shows the statistics of evaluation failures under the conventional *K*-method, which does not occur in the proposed method.

It can be seen from the Table III that, in the daily evaluation of AGC units, the cumulative time of evaluation failures caused by conventional method reached tens or even hundreds of hours, which brings quite expensive economic penalties to the AGC power plants. To solve this problem, it is recommended to optimize the set-point power issued by the dispatching center, which is the follow-up research direction of this study.

5. Conclusion

AGC performance evaluation in power system is essential to realize real-time energy balance in power system. It is necessary for the dispatch center to confirm the optimal performance of AGC units to improve the rationality of the instructions.

According to the experimental results and analysis, it is discovered that after the single dynamic interval segmentation of AGC-related data, a sample space reflecting the tracking ability of the AGC unit could be constructed, and the data preprocessing and data cleaning further highlight the distribution characteristics. Thus, the optimal operation points of AGC units could be found by fitting AGC samples under different feature dimensions. For thermal AGC units, the time to reach the optimal performance increases with the amplitude of the AGC instructions. Furthermore, the proposed method visually distinguishes the difficulty of AGC tasks. According to the data-driven evaluation, different AGC units have their customary regulation power in daily operation. In addition, the proposed method solves the problem of evaluation failure in traditional methods.

To sum up, the proposed method demonstrates competitive capabilities in AGC evaluation. It provides a theoretical basis for the combination of data-driven analysis and AGC performance evaluation, which is conducive to accurate power dispatching.

AGC is mainly used to solve the imbalance of power supply and demand in the energy system, while large-scale renewable energy, such as wind power, is the main reason for power supply fluctuations. Therefore, as the future research direction, the short-term wind power prediction of renewable energy will be combined with the evaluation of AGC performance. In addition, in order to ensure the safety and stability of the wind and thermal power bundled energy system, it is necessary to achieve more accurate AGC control of thermal power units and work with the AGC of renewable energy stations to jointly ensure the safe and economic operation of the grid.

CRediT authorship contribution statement

Bin Li: Conceptualization, Funding acquisition, Writing – review & editing. **Shuai Wang:** Methodology, Software, Validation, Writing- original draft. **Botong Li:** Project administration. **Hongbo Li:** Resources, Investigation, Formal analysis. **Jianzhong Wu:** Supervision, Writing – review & editing.

Declaration of Competing Interest

The authors declare that they have no known competing financial interests or personal relationships that could have appeared to influence the work reported in this paper.

Acknowledgments

This work was supported by Science and Technology Project of State Grid Corporation of China (Research and application of audiovisual active perception and collaborative cognitive technology for smart grid operation and maintenance scenarios) (5600-202046347 A-0-0-00).

References

[1] Xi L, Sun MM, Zhou H, Xu YC, Wu JN, Li YY. Multi-agent deep reinforcement learning strategy for distributed energy. Measurement 2021;185: 109955.

[2] Pathak N, Bhatti TS, Verma A, Nasiruddin I. AGC of Two Area Power System Based on Different Power Output Control Strategies of Thermal Power Generation. IEEE Transactions on Power Systems 2018;33(2):2040-2052.

[3] Xi L, Wu JN, Xu, YC, Sun HB. Automatic Generation Control Based on Multiple Neural Networks With Actor-Critic Strategy. IEEE Transactions on Neural Networks and Learning Systems 2021;32(6):2483-2493.

[4] Farooq U, Bass RB. Frequency Event Detection and Mitigation in Power Systems: A Systematic Literature Review 2022;10: 61494-61519.

[5] Rebours YG, Kirschen DS, Trotignon M, Rossignol S. A survey of frequency and voltage control ancillary services - Part I: Technical features. IEEE Transactions on Power Systems 2007;22(1):350-357.

[6] Xi L, Zhang ZY, Yang B, Huang LN, Yu Tao. Wolf pack hunting strategy for automatic generation control of an islanding smart distribution network. Energy Conversion and Management 2016;122:10-24.

[7] Rebours YG, Kirschen DS, Trotignon M, Rossignol S. A survey of frequency and voltage control ancillary services - Part II: Economic features. IEEE Transactions on Power Systems 2007;22(1):358-366.

[8] Xu BL, Dvorkin Y, Kirschen DS, Silva-Monroy CA, Watson JP.A Comparison of Policies on the Participation of Storage in US Frequency Regulation Markets. in Proc. IEEE Power Energy Soc. Gen. Meeting 2016:1-5.

[9] Chen XS, Lin J, Liu F, Song YH. Optimal Control of AGC Systems Considering Non-Gaussian Wind Power Uncertainty. IEEE Transactions on Power Systems 2019;34(4):2730-2743.

[10] Xi L, Zhou LP, Xu YC, Chen X. A Multi-Step Unified Reinforcement Learning Method for Automatic Generation Control in Multi-Area Interconnected Power Grid. IEEE Transactions on Sustainable Energy 2021;12(2): 1406-1415.

[11] Ganger D, Zhang JS, Vittal V. Forecast-Based Anticipatory Frequency Control in Power Systems. IEEE Transactions on Power Systems 2018; 33(1):1004-1012.

[12] Badu NR, Saikia LC. Load frequency control of a multi-area system incorporating realistic high-voltage direct current and dish-Stirling solar thermal system models under deregulated scenario. IET Renewable Power Generation 2021;15(5): 1116-1132.

[13] Shen JJ, Hu L, Cheng CT, Wang S. Automatic generation control of a large hydropower plant with head-sensitive forbidden and restricted zones. IET Renewable Power Generation2020;14(7):1113-1123.

[14] Dong Z, Liu M, Zhang ZY, Dong YJ, Huang XJ. Automatic generation control for the flexible operation of multimodular high temperature gas-cooled reactor plants. Renewable and Sustainable Energy Reviews 2019;108:11-31.

[15] Donadee J, Wang JH. AGC Signal Modeling for Energy Storage Operations. IEEE Transactions on Power Systems 2014;29(5):2567-2568.

[16] Delille G, Francois B, Malarange G. Dynamic Frequency Control Support by Energy Storage to Reduce the Impact of Wind and Solar Generation on Isolated Power System's Inertia. IEEE Transactions on Sustainable Energy2012;3(4):931-939.

[17] Latif A, Hussain SMS, Das DC, Ustun TS. State-of-the-art of controllers and soft computing techniques for regulated load frequency management of single/multi-area traditional and renewable energy based power systems. Applied Energy 2020;266:114858.

[18] Chen XS, Lin J, Liu F, Song YH. Stochastic Assessment of AGC Systems Under Non-Gaussian Uncertainty. IEEE Transactions on Power Systems 2019;34(1):705-717.

[19] Egido I, Fernandez-Bernal F, Rouco L. The Spanish AGC System: Description and Analysis. IEEE Transactions on Power Systems 2009;24(1):271-278.

[20] PJM, Docket No. ER12-1204-001, Mar. 5, 2012 [Online]. Available: http://www.pjm.com/~/media/documents/ferc/2012-filings/20120305-er12-1204-000.ashx.

[21] Zeng M, Liu XM, Peng LL. The ancillary services in China: An overview and key issues. Renewable & Sustainable Energy Reviews 2014;36:83-90.

[22] Chakraborty T, Watson D, Rodgers M. Automatic Generation Control Using an Energy Storage System in a Wind Park. IEEE Transactions on Power Systems 2018;33(1):198-205.

[23] Zhang XS, Xu Z, Yu T, Yang B. Wang HZ. Optimal Mileage Based AGC Dispatch of a GenCo. IEEE Transactions on Power Systems 2020;35(4):2516-2526.

[24] Doenges K, Egido I, Sigrist L, Miguelez EL, Rouco L. Improving AGC Performance in Power Systems with Regulation Response Accuracy Margins Using Battery Energy Storage System (BESS). IEEE Transactions on Power Systems 2020;35(4):2816-2825.

[25] 50Hertz Transmission GmbH, Amprion GmbH, TenneT TSO GmbH, TransnetBW GmbH, "MarktinformationAnpassungung der Abrechnungsbedingungen für Sekundärregelarbeit," 2018. [Online]. Available: https://www.regelleistung.net/ext/download/Konsultation_SRL_Abrechnung

[26] Egido I, Fernandez-Bernal F, Rouco L. Evaluation of Automatic Generation Control (AGC) regulators by performance indices using data from real operation. IET Generation Transmission & Distribution 2007;1(2):294-302.

[27] Xi L, Zhang L, Liu JC, Li YD, Chen X, Yang LQ, Wang SX. A Virtual Generation Ecosystem Control Strategy for Automatic Generation Control of Interconnected Microgrids. IEEE Access 2020;8: 94165-94175.

[28] Liu LK, Hu ZC, Mujeeb, A. Automatic Generation Control Considering Uncertainties of the Key Parameters in the Frequency Response Model. IEEE Transactions on Power Systems 2022;37(6): 4605-4617.

[29] Magzoub MA, Alquthami T. Optimal Design of Automatic Generation Control Based on Simulated Annealing in Interconnected Two-Area Power System Using Hybrid PID-Fuzzy Control. Energies 2022;15(4):1540.

[30] Fan L, Zhao CY, Zhang GY, Huang QH. Flexibility Management in Economic Dispatch With Dynamic Automatic Generation Control. IEEE Transactions on Power Systems 2022;37(2): 876-886.

[31] Kumar V, Sharma V, Naresh R. Leader Harris Hawks algorithm based optimal controller for automatic generation control in PV-hydro-wind integrated power network. Electric Power Systems Research 2022;214(B):108924.

[32] Li JW, Yu T, Zhang XS, Li FS, Lin D, Zhu HX. Efficient experience replay based deep deterministic policy gradient for AGC dispatch in integrated energy system. Applied Energy 2021;285:116386.

[33] Badu NR, Bhagat SK, Saikia LC, Chiranjeevi T, Devarapalli R, Marquez FPG. A Comprehensive Review of Recent Strategies on Automatic Generation Control/Load Frequency Control in Power Systems 2022; [Online]. Available: https://link.springer.com/article/10.1007/s11831-022-09810-y.

[34] Ozer B, Arikan O, Moral G, Altintas A. Extraction of primary and secondary frequency control from active power generation data of power plants. International Journal of Electrical Power & Energy Systems 2015;73:16-22.

[35] Egido I, Fernandez-Bernal F, Rouco L, Porras E,Saiz-Chicharro A. Modeling of Thermal Generating Units for Automatic Generation Control Purposes. IEEE Transactions on Control Systems Technology 2004;12(1):205-210.

[36] Bondy DEM, Thavlov A, Tougaard JBM, Heussen K. Performance requirements modeling and assessment for active power ancillary services. 2017 IEEE Manchester PowerTech, 1–6, Manchester, UK, June 18–22. 2017.

[37] Wang JD, Pang XK, Gao S, Zhao Y, Cui SJ. Assessment of automatic generation control performance of power generation units based on amplitude changes. International Journal of Electrical Power & Energy Systems 2019;108:19-30.

[38] Xi L, Li HK, Zhu JZ, Li YY, Wang SX. A Novel Automatic Generation Control Method Based on the Large-Scale Electric Vehicles and Wind Power Integration Into the Grid. IEEE Transactions on Neural Networks and Learning Systems 2022[Online]. Available: https://ieeexplore.ieee.org/stamp/stamp.jsp?tp=&arnumber=9851222.

[39] Xi L, Zhang L, Xu YC, Wang SX, Yang C. Automatic Generation Control Based on Multiple-step Greedy Attribute and Multiple-level Allocation Strategy. CSEE Journal of Power and Energy Systems 2022;8(1):281-292.

[40] Xi L, Yu L, Xu YC, Wang SX, Chen X. A Novel Multi-Agent DDQN-AD Method-Based Distributed Strategy for Automatic Generation Control of Integrated Energy Systems. IEEE Transactions on Sustainable Energy 2020;11(4):2417-2426.

[41] Chen CY, Chen Y, Zhao JB, Zhang KF, Ni M, Ren BX. Data-Driven Resilient Automatic Generation Control Against False Data Injection Attacks. IEEE Transactions on Industrial Informatics 2021;17(12):8092-8101.

[42] Rodriguez A, Laio A. Clustering by fast search and find of density peaks. Science 2014;344(6191):1492-6.